Vacancy-Impurity Complexes in Highly Sb-Doped Si Grown by Molecular Beam Epitaxy

M. Rummukainen, I. Makkonen, V. Ranki, M. J. Puska, and K. Saarinen
Laboratory of Physics, Helsinki University of Technology, P.O. Box 1100, FIN-02015 HUT, Finland

H.-J. L. Gossmann
Axcelis Technologies, Beverly, Massachusetts 01915, USA

(Received 23 July 2004; published 25 April 2005)

Positron annihilation measurements, supported by first-principles electron-structure calculations, identify vacancies and vacancy clusters decorated by 1–2 dopant impurities in highly Sb-doped Si. The concentration of vacancy defects increases with Sb doping and contributes significantly to the electrical compensation. Annealings at low temperatures of 400–500 K convert the defects to larger complexes where the open volume is neighbored by 2–3 Sb atoms. This behavior is attributed to the migration of vacancy-Sb pairs and demonstrates at atomic level the metastability of the material grown by epitaxy at low temperature.

DOI: 10.1103/PhysRevLett.94.165501 PACS numbers: 61.72.-y, 61.82.Fk, 78.70.Bj

The interest in highly doped Si is fundamentally related to the miniaturization of field-effect transistors, where increased doping is needed to maintain a sufficient conductance of the source and drain regions [1]. The free electron concentration in n-type Si, however, has been found to saturate at $<5 \times 10^{20}$ cm^{-3} regardless of the doping density [2,3]. This electrical deactivation has been attributed to the formation of point defects. The presence of vacancy-impurity complexes such as $V - As_3$ has been verified in melt-grown or ion-implanted material [4–6], and their formation has been explained by kinetic migration processes [7].

The molecular beam epitaxy (MBE) growth at low temperature (< 600 K) can be applied to achieve metastable doping and free electron concentrations, which become compensated only at 10^{21} cm^{-3} [8]. At these very high doping levels the pairing of impurities may happen due to purely statistical reasons [9,10]. The electron microscopy studies have, indeed, observed donor pairs at concentrations expected for compensating defects [10,11]. These donor pairs (DP) have recently been attributed to the configuration $DP - V - I$, where the Si atom neighboring the Sb dopant pair has relaxed towards the interstitial site (I) leaving a vacancy (V) behind [11]. The presence and size of the open volume in this defect has been deduced indirectly by comparing the positions of the Sb atoms to the theoretically predicted lattice relaxation [11]. On the other hand, the positron annihilation experiments of Szpala *et al.* suggest that open-volume defects larger than monovacancies may be present [12].

In this work we apply positron annihilation spectroscopy to study vacancies formed in the low-temperature MBE growth of highly Sb-doped Si. Positrons get trapped at open-volume defects. The measured annihilation photons carry information on the electron momentum density, which can be utilized to identify the size of the open volume of the defect and the neighboring dopant atoms. Our results show that the MBE growth creates vacancies and vacancy clusters, which are neighbored by 1–2 Sb atoms. The vacancy concentrations are relevant for the compensation of the Sb doping. We also show that the low-temperature MBE Si is atomically metastable, and annealings at low temperatures of 400–500 K lead to clustering of vacancies and dopant impurities.

We studied Si(100) layers grown by MBE on the Si substrate at 550 K (Table I) [8]. Sample No. 1 with the largest doping concentration was electrically highly compensated (fraction of free electron concentration n to [Sb] ~ 0.06) while the three other samples were more active ($n/[\mathrm{Sb}] > 0.7$). The native surface oxide was removed by HF etching. The samples are the same as those used in the previous electron microscopy experiments [10,11]. As a reference material we studied bulk Si(111) samples with $[\mathrm{Sb}] = 3 \times 10^{18}$ cm^{-3} before and after 2 MeV electron irradiation at 300 K with a fluence of 3×10^{17} cm^{-2}.

We used a low-energy positron beam to measure the Doppler broadened energy spectrum of the annihilation radiation. The shape of the spectrum was described with conventional S and W parameters [13], representing the fractions of annihilations with low momentum (valence) electrons and high momentum (core) electrons, respectively. Measurements were made also using a coincidence of two Ge detectors (energy resolution of 0.92 keV) [13].

TABLE I. Thicknesses Th, and Sb doping and free electron concentrations n of the samples. The positron diffusion lengths L and total vacancy concentrations $[V]$ were obtained from the analysis of positron annihilation results.

Sample	Th (nm)	[Sb] (cm^{-3})	n (cm^{-3})	L (nm)	$[V]$ (cm^{-3})
No. 1	30	3.7×10^{21}	2.3×10^{20}	4(1)	$9(3) \times 10^{20}$
No. 2	70	9.4×10^{20}	6.5×10^{20}	9(2)	$1.5(5) \times 10^{20}$
No. 3	50	5.9×10^{20}	4.2×10^{20}	16(3)	$5(2) \times 10^{19}$
No. 4	30	2.7×10^{19}	2.4×10^{19}	≥ 30	$\leq 10^{19}$

We modeled positron annihilation parameters using electronic-structure calculations. A supercell of 64 atomic sites was used to describe defects where the atoms occupied the ideal lattice sites. Only the neutral defect states were considered. The valence electron densities were calculated self-consistently using the local-density approximation (LDA) employing the projector augmented-wave (PAW) method [14] and the plane-wave code VASP [15,16]. Atomic wave functions were used for core electrons. The positron states and annihilation characteristics were calculated within the LDA and the state-dependent enhancement scheme [17,18]. We constructed all-electron valence wave functions within the PAW method for calculating the momentum distributions [19], which were finally convoluted with the resolution of the Doppler experiment.

The S parameter as a function of positron implantation energy E is shown in Fig. 1. The S parameter is sensitive to surface effects at $E < 0.3$ keV. Already at $E = 3$ keV almost all annihilations take place in the substrate. The S parameter increases with doping at the depth corresponding to the highly Sb-doped layer at $E = 0.5$ keV. The $S(E)$ peaks in samples No. 1 and No. 2 show that the electron density is reduced and indicate high vacancy densities in the Sb-doped layer. The vacancies form open-volume clusters at least in sample No. 1, since $S/S_B = 1.08$ is much higher than expected for monovacancies [13].

The sharp peaks of S parameters in the thin layers No. 1 and No. 2 indicate that the positron diffusion lengths L are smaller than the layer thicknesses or the value of $L_B = 220$ nm in the defect-free Si lattice. The diffusion lengths can easily be estimated in samples where the thin (<1 nm) native surface oxide was not removed by etching. The oxide decreases the S parameter at the surface to smaller values than in the layer or the substrate (inset of Fig. 1). Assuming a homogeneous layer with the thicknesses of Table I, the positron backdiffusion probability to the oxide can be fitted to the $S(E)$ data to determine the diffusion length [13]. The positron trapping rate can be obtained as $\kappa \approx (L_B/L)^2 \times \lambda_B$, where $\lambda_B = 4.5\ \mathrm{ns}^{-1}$ is the positron annihilation rate in the lattice. The total concentration of vacancy defects limiting positron diffusion by trapping is simply $[V] = \kappa/\mu$, where we use the positron trapping coefficient $\mu = 10^{15}\ \mathrm{s}^{-1}$. The estimated concentrations are in the $10^{20}\ \mathrm{cm}^{-3}$ range (Table I), and thus are very significant for the compensation of the Sb doping.

In order to identify the defects formed in the growth of highly Sb-doped Si, we applied electron irradiation to create reference samples containing high concentrations of $V-\mathrm{Sb}$ and $V-\mathrm{Sb}_2$. The irradiation-induced vacancy migrates until trapped by the impurity atom to form E centers such as $V-\mathrm{Sb}$ and $V-\mathrm{P}$ (see, e.g., Refs. [20,21] and references therein). The $V-\mathrm{Sb}$ pairs can be converted to $V-\mathrm{Sb}_2$ by migration at 600 K [7,20]. The electron momentum distributions are shown in Fig. 2 as ratios to the measured data of the $V-\mathrm{P}$ pair. This scaling is useful since the $V-\mathrm{P}$ pair has a similar core electron momentum density as the isolated Si vacancy [5], and thus the ratio emphasizes the vacancy decoration by Sb atoms.

The measured ratio curve in the $V-\mathrm{Sb}$ pair is constant and equal to unity at the low momenta of $(0\text{–}5) \times 10^{-3} m_0 c$ (m_0 is the free electron mass and c is the speed of light). This indicates, as expected, that the valence electron momentum densities are similar at the $V-\mathrm{P}$ and $V-\mathrm{Sb}$ pairs. At $(10\text{–}20) \times 10^{-3} m_0 c$ the ratio curve forms a broad

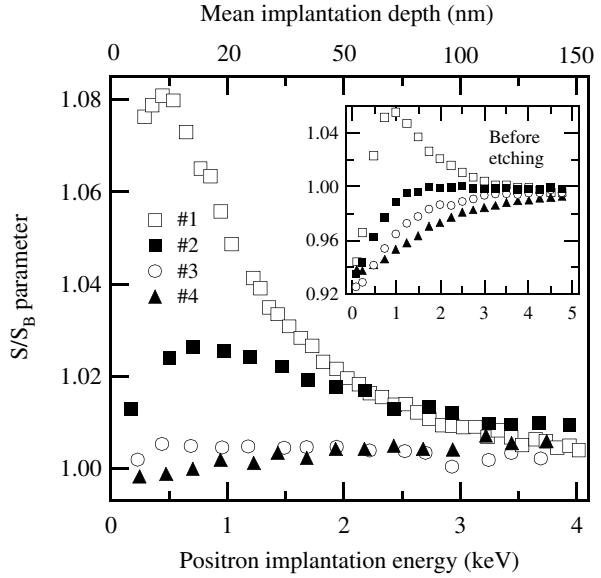

FIG. 1. S parameter vs positron implantation energy, converted to the mean stopping depth in the top axis. The S parameter is scaled to the bulk lattice value S_B obtained in the substrate. The inset shows the results in samples with the native oxide on the surface.

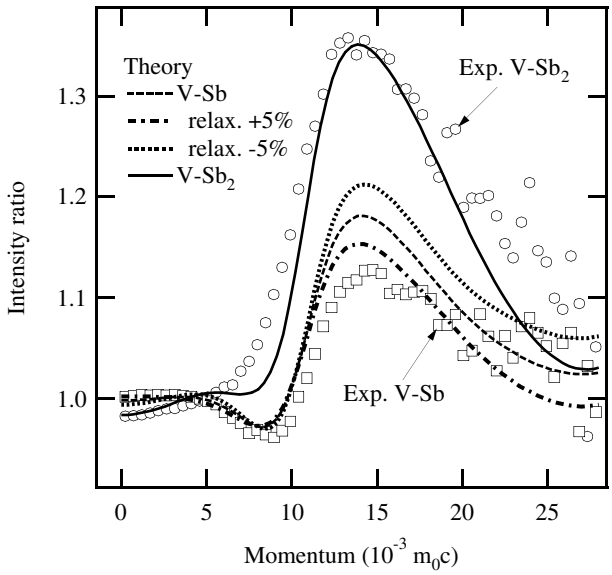

FIG. 2. The momentum density along the [111] direction at the irradiation-induced $V-\mathrm{Sb}$ and $V-\mathrm{Sb}_2$ defects, as scaled to that of the $V-\mathrm{P}$ pair. The lines are obtained from theoretical calculations, showing also the influence of lattice relaxation (fraction of the Si-Si bond length, Sb atoms relaxed only).

peak, which is due to the 4*d* electrons of the Sb atoms. The peak is about twice as intense in the ratio curve of the $V - Sb_2$ complex, due to two Sb atoms neighboring the vacancy. The momentum ratio to the $V - P$ pair decreases below unity in the $V - Sb_2$ complex at $(0–5) \times 10^{-3} m_0 c$. This effect has been observed before [5,20], and can be traced back to the pileup of the electron density around positive Sb donors, resulting in an increase of the valence electron momenta.

The calculated ratio curves are in good agreement with experiments at $(0–5) \times 10^{-3} m_0 c$ (Fig. 2) indicating the correct theoretical description of the valence electron momentum density. The intensity of the peak at $(10–20) \times 10^{-3} m_0 c$ reflects the increase of annihilations with the Sb 4*d* electrons. Much of the remaining discrepancy can be associated with the lattice relaxations around the defects, as demonstrated by calculations in Fig. 2.

The defects formed in the MBE growth were studied especially in sample No. 2, since this doping concentration was investigated most carefully also by electron microscopy [10,11]. Figure 3 shows the measured electron momentum density in the [100] direction, shown again as scaled to that of a $V - P$ pair (along the [111] direction). The valence electron region has a narrower momentum density than in the $V - P$ pair, as manifested by the increase of the momentum ratio above unity at $(0–2) \times 10^{-3} m_0 c$. The ratio curve increases up to 1.2 and forms a broad peak at $(10–20) \times 10^{-3} m_0 c$. The broad flat peak in contrast to the sharper peak in Fig. 2 is due to the two different directions used in the ratio. As explained above for the $V - Sb$ pair and the $V - Sb_2$ complex, the peak indicates that the vacancy defect is surrounded by Sb atoms.

The comparison to theoretical calculations shows that no single defect type is able to explain the experimental ratio curve at all momenta (Fig. 3). Several important conclusions can be made, however, by comparing the relevant parts of the curves. First, the narrowing of the momentum density at $(0–3) \times 10^{-3} m_0 c$ indicates that divacancies are present, since Sb-decorated monovacancies lead to momentum ratios below unity. In fact, at $(0–5) \times 10^{-3} m_0 c$ the experimental curve is very similar to that calculated for $V_2 - Sb_2$. Second, the broad peak at $(10–20) \times 10^{-3} m_0 c$ due to Sb 4*d* electrons is much better reproduced by monovacancy complexes $V - Sb$ and $V - Sb_2$ than by the decorated divacancies. The best agreement is obtained for the $V - Sb$ pair. Third, the calculations show that positrons are only weakly localized at the donor pair defects in both configurations $DP(2) - V - I$ and $DP(4) - V - I$ (defined in Ref. [11]). The ratio curve (Fig. 3) is similar for both configurations and does not agree with the experimental data at any momentum range.

The experimental momentum density of defects trapping positrons in highly Sb-doped Si can thus be constructed of a superposition of monovacancies and divacancies surrounded by 1–2 Sb atoms. These vacancy-Sb complexes have high concentrations (Table I) and are thus important for the compensation of Sb donors. Our result

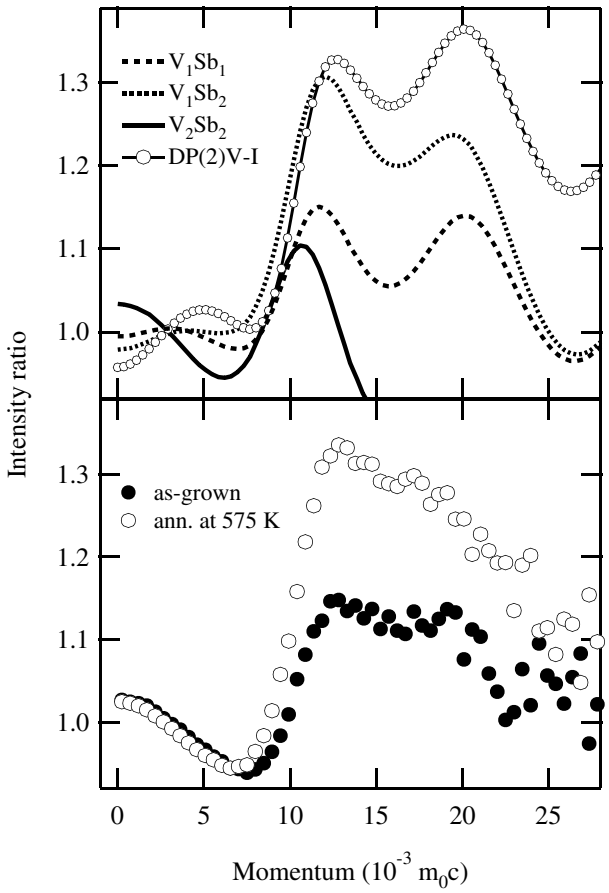

FIG. 3. Momentum density of the vacancy defect in the as-grown Sb-doped Si (sample No. 2) and after annealing at 575 K. The measured momentum density along the [100] direction is scaled to that of the $V - P$ pair along the [111] axis, leading to oscillations. The lines in the upper panel are obtained from theoretical calculations in various model structures.

is in agreement with the electron microscopy studies [10], where Sb impurities appear either in isolation or in pairs. The theoretical donor pair defects DP2, DP4, and $DP - V - I$ [9,11] have a much too small open volume and high electron density to be compatible with our experimental positron data.

The detected donor pair in electron microscopy is attributed to the $DP - V - I$ structure on the basis on theoretically calculated relaxed positions of the Sb atoms [11]. The $V - Sb_2$ complex was rejected in the analysis because the LDA calculation resulted in a too large inwards relaxation of the Sb atoms neighboring the vacancy [11]. The results in Fig. 2 show that calculations in the ideal or slightly outward relaxed structures can explain the experimental data obtained in the $V - Sb$ and $V - Sb_2$ complexes produced by the electron irradiation. These findings provide a challenge to the theoretical calculations of the atomic structures and may require reinterpretation of the electron microscopy images in Refs. [10,11].

The presence of defects like $V - Sb_2$ and $V_2 - Sb_2$ is compatible with diffusion data. According to electron ir-

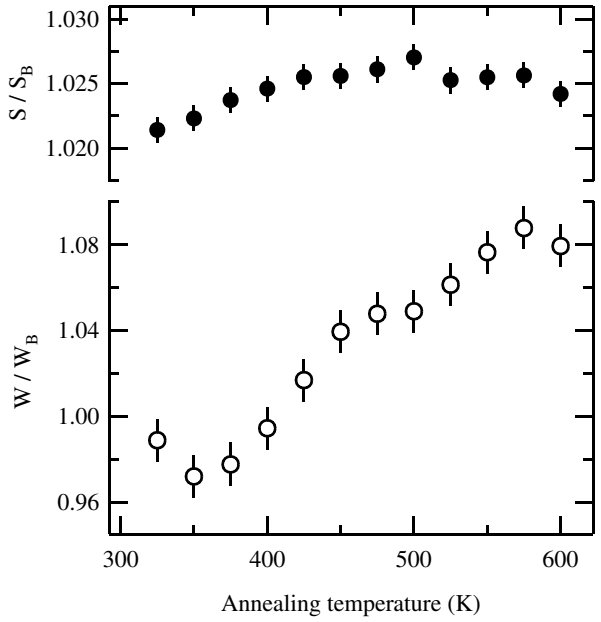

FIG. 4. S and W parameters (measured at 300 K, positron energy 1 keV, sample No. 2) vs annealing temperature. The parameters are scaled to their lattice values S_B and W_B.

radiation studies [20], the $V-\mathrm{Sb}$ pair is mobile at the growth temperature of 550 K. Its migration leads thus to the formation of more stable complexes like $V-\mathrm{Sb}_2$ and $V_2-\mathrm{Sb}_2$ when encountering an isolated Sb atom or another $V-\mathrm{Sb}$ pair. The $V-\mathrm{Sb}_2$ complex is stable up to 700 K [20], which is above the growth temperature of the present material. Hence, no vacancy complexes with three donor impurities can form, although such defects are prominent in Si grown from the melt or by MBE above 700 K [5,6]. The vacancy migration processes thus give a microscopic explanation to the higher fraction of electrically active Sb dopants in MBE samples grown at low temperature.

The thermal stability of vacancies in highly Sb-doped Si is studied in Fig. 4. The W parameter increases significantly during annealings at 300–600 K. The same effect is seen in Fig. 3, which shows that the contribution of Sb $4d$ electrons increases strongly. The comparison with theoretically calculated curves (Fig. 3) indicates that after 600 K heat treatment the monovacancies and divacancies are neighbored by 2–3 Sb atoms. The slight increase of the S parameter (Fig. 4) suggests further that the vacancy clusters grow in size. We attribute these effects to the clustering induced by the $V-\mathrm{Sb}$ pair, which becomes mobile at 400–500 K. The highly Sb-doped MBE Si is thus atomically metastable after the growth; the grown-in vacancies mediate the formation of larger vacancy-Sb clusters by annealing already below the growth temperature.

The presence of vacancies in low-temperature grown MBE Si may be surprising, since the vacancy formation energy is high according to theoretical calculations (3.8 eV in Ref. [9]). However, in highly doped material the vacancy-impurity complexes may form much more abundantly since their formation energy is decreased by the strong binding between the vacancy and the donor atoms. For example, the formation energies of neutral $V-\mathrm{Sb}$ and $V-\mathrm{Sb}_2$ are 2.5 and 0.8 eV, respectively [9]. Furthermore, the low-temperature MBE growth does not take place in thermal equilibrium and the vacancy concentration may be supersaturated due to kinetic processes at the surface. Such large vacancy concentrations have been observed also in the low-temperature MBE growth of GaAs [22].

To conclude, our positron annihilation measurements, supported by theoretical predictions, show the formation of vacancies and vacancy clusters in highly Sb-doped Si grown by molecular beam epitaxy. The open-volume defects are neighbored by 1–2 Sb impurities, and their concentration is large enough to be important for the electrical deactivation of Sb doping. Annealing experiments show that vacancy defects are unstable already at 400–500 K and form larger vacancy-Sb complexes, most likely by the migration of $V-\mathrm{Sb}$ pairs. The results demonstrate the metastable nature of Sb doping in Si grown by low-temperature MBE and explain the high electrical activation of Sb and deactivation in annealing by kinetic migration processes of vacancy defects.

[1] P. A. Packan, Science **285**, 2079 (1999).
[2] A. Lietoila, J. F. Gibbons, and T. W. Sigmon, Appl. Phys. Lett. **36**, 765 (1980).
[3] P. M. Fahey, P. B. Griffin, and J. D. Plummer, Rev. Mod. Phys. **61**, 289 (1989).
[4] D. W. Lawther *et al.*, Appl. Phys. Lett. **67**, 3575 (1995).
[5] K. Saarinen *et al.*, Phys. Rev. Lett. **82**, 1883 (1999).
[6] V. Ranki *et al.*, Phys. Rev. B **67**, 041201 (2003).
[7] V. Ranki, J. Nissilä, and K. Saarinen, Phys. Rev. Lett. **88**, 105506 (2002).
[8] H.-J. Gossmann, F. C. Unterwald, and H. S. Luftman, J. Appl. Phys. **73**, 8237 (1993).
[9] D. J. Chadi *et al.*, Phys. Rev. Lett. **79**, 4834 (1997).
[10] P. M. Voyles *et al.*, Nature (London) **416**, 826 (2002).
[11] P. M. Voyles *et al.*, Phys. Rev. Lett. **91**, 125505 (2003).
[12] S. Szpala *et al.*, Phys. Rev. B **54**, 4722 (1996).
[13] R. Krause-Rehberg and H. S. Leipner, *Positron Annihilation in Semiconductors* (Springer, New York, 1999).
[14] P. E. Blöchl, Phys. Rev. B **50**, 17 953 (1994).
[15] G. Kresse and J. Furthmüller, Phys. Rev. B **54**, 11 169 (1996).
[16] G. Kresse and D. Joubert, Phys. Rev. B **59**, 1758 (1999).
[17] We use the parametrization by E. Boronski and R. M. Nieminen, Phys. Rev. B **34**, 3820 (1986).
[18] M. Alatalo *et al.*, Phys. Rev. B **54**, 2397 (1996).
[19] I. Makkonen, M. Hakala, and M. J. Puska, J. Phys. Chem. Solids (to be published).
[20] V. Ranki, A. Pelli, and K. Saarinen, Phys. Rev. B **69**, 115205 (2004).
[21] V. Avalos and S. Dannefaer, Phys. Rev. B **58**, 1331 (1998).
[22] J. Gebauer *et al.*, Appl. Phys. Lett. **79**, 4313 (2001).